Mon. Not. R. Astron. Soc. **364,** 620–634 (2005) doi:10.1111/j.1365-2966.2005.09583.x

Statistical analysis of galaxy surveys – II. The three-point galaxy correlation function measured from the 2dFGRS

E. Gaztañaga,[1,2⋆] P. Norberg,[3] C. M. Baugh[4] and D. J. Croton[5]

[1] *Instituto de Ciencias del Espacio (IEEC/CSIC), F. de Ciencies UAB, Torre C5- Par- 2a, Bellaterra, 08193 Barcelona, Spain*
[2] *INAOE, Astrofisica, Tonantzintla, Puebla 7200, Mexico*
[3] *ETHZ Institut für Astronomie, HPF G3.1, ETH Hönggerberg, CH-8093 Zürich, Switzerland*
[4] *Department of Physics, University of Durham, South Road, Durham DH1 3LE*
[5] *Max-Planck-Institut für Astrophysik, D-85740 Garching, Germany*

Accepted 2005 September 1. Received 2005 September 1; in original form 2005 June 16

ABSTRACT

We present new results for the three-point correlation function, ζ, measured as a function of scale, luminosity and colour from the final version of the 2dF Galaxy Redshift Survey (2dFGRS). The reduced three-point correlation function, $Q_3 \sim \zeta/\xi^2$, is estimated for different triangle shapes and sizes, employing a full covariance analysis. The form of Q_3 is consistent with the expectations for the Λ cold dark matter model, confirming that the primary influence shaping the distribution of galaxies is gravitational instability acting on Gaussian primordial fluctuations. However, we find a clear offset in amplitude between Q_3 for galaxies and the predictions for the dark matter. We are able to rule out the scenario in which galaxies are unbiased tracers of the mass at the 9σ level. On weakly non-linear scales, we can interpret our results in terms of galaxy bias parameters. We find a linear bias term that is consistent with unity, $b_1 = 0.93^{+0.10}_{-0.08}$ and a quadratic bias $c_2 = b_2/b_1 = -0.34^{+0.11}_{-0.08}$. This is the first significant detection of a non-zero quadratic bias, indicating a small but important non-gravitational contribution to the three-point function. Our estimate of the linear bias from the three-point function is independent of the normalization of underlying density fluctuations, so we can combine this with the measurement of the power spectrum of 2dFGRS galaxies to constrain the amplitude of matter fluctuations. We find that the rms linear theory variance in spheres of radius $8\,h^{-1}$ Mpc is $\sigma_8 = 0.88^{+0.12}_{-0.10}$, providing an independent confirmation of values derived from other techniques. On non-linear scales, where $\xi > 1$, we find that Q_3 has a strong dependence on scale, colour and luminosity.

Key words: galaxies: statistics – cosmology: theory – large-scale structure of Universe.

1 INTRODUCTION

The higher-order statistics of galaxy clustering encode fundamental information about two key dynamical aspects of the large-scale structure of the Universe: the growth mechanism of fluctuations and the connection between the galaxy distribution and the underlying mass (for a review, see Bernardeau et al. 2002). An accurate measurement of the three-point correlation function of galaxies has the potential to test the gravitational instability paradigm of structure formation and, on scales that are evolving in the weakly non-linear regime, to separate the effects of gravity from the contributions arising from galaxy bias (Fry & Gaztañaga 1993; Frieman & Gaztañaga 1994).

The measurement of the three-point function and other higher-order statistics from galaxy catalogues has a rich history (Peebles & Groth 1975; Groth & Peebles 1977; Fry & Peebles 1978; Baumgart & Fry 1991; Gaztañaga 1992; Bouchet et al. 1993; Fry & Gaztañaga 1994). In the past decade, three-point statistics have supported the basic premise of gravitational instability from Gaussian initial conditions (Frieman & Gaztañaga 1994; Jing & Börner 1998; Frieman & Gaztañaga 1999; Hoyle, Szapudi & Baugh 2000; Feldman et al. 2001). The impact of these measurements on theoretical models has, however, not been as great as it could have been for two reasons. First, the traditional theoretical predictions rely upon the application of perturbation theory, which limits the comparison with data to relatively large scales on which the fluctuations are evolving in a linear or weakly non-linear fashion. Secondly, previous generations of galaxy surveys simply covered too little volume to permit accurate measurements of the higher-order correlation functions on the scales that could strongly constrain the simple theoretical models.

Recent theoretical and observational advances have been such that we are now in a position to realize the full potential of

⋆E-mail: gazta@ieec.fcr.es

© 2005 The Authors. Journal compilation © 2005 RAS

higher-order statistics. Theoretical models of galaxy formation have progressed sufficiently to make predictions for the number of galaxies that reside in dark matter haloes of different mass (Benson et al. 2000; Peacock & Smith 2000; Scoccimarro et al. 2001b; Berlind et al. 2003). This allows the prediction to be extended to scales for which perturbation theory is not valid, and provides a framework for testing the physics of galaxy formation directly against clustering measurements. Observationally, two recent surveys have revolutionized our view of the local Universe: the 2dF Galaxy Redshift Survey (2dFGRS; Colless et al. 2001) and the Sloan Digital Sky Survey (SDSS; York et al. 2000). The tenfold increase in survey size achieved by these projects means that precision measurements of higher-order statistics are now possible across a range of scales (Matarrese, Verde & Heavens 1997; Colombi, Szapudi & Szalay 1998; Szapudi, Colombi & Bernardeau 1999; Scoccimarro, Sefusatti & Zaldarriaga 2004; Sefusatti & Scoccimarro 2005). The higher-order clustering measurements that are possible with these surveys have the potential to tighten the accepted values of basic cosmological parameters and to constrain the physics of galaxy formation that govern how galaxies are clustered.

There have have been several analyses of the distribution of counts-in-cells using the final 2dFGRS catalogue. Baugh et al. (2004) demonstrated that the higher-order correlation functions display a hierarchical scaling, $S_p = \bar{\xi}_p/\bar{\xi}_2^{p-1}$, where $\bar{\xi}_p$ is the p-point, volume-averaged correlation function; this behaviour is expected if gravity plays a dominant role in shaping the distribution of galaxies. Croton et al. (2004b) found that the scaling of the hierarchical coefficients shows a weak (if any) dependence on galaxy luminosity. In the case of the three-point volume-averaged correlation function, both authors found that the skewness, $S_3 = \bar{\xi}_3/\bar{\xi}_2^3 \simeq 2$. This value was found to be independent of cell size, although both Baugh et al. and Croton et al. noted that two large superstructures in the 2dFGRS volume broke this scale invariance in catalogues characterized by $L_\star$ galaxies. The result for the skewness of galaxies, $S_3 \simeq 2$, is at odds with the expectation for a Λ cold dark matter (CDM) cosmology, in which $S_3^{\rm DM} \simeq 3$. We note that Conway et al. (2005) and Wild et al. (2005) have also looked at the constraints that the distribution of counts-in-cells in the 2dFGRS provide on galaxy bias. All results from the 2dFGRS are in line with most previous measurements of the skewness and three-point statistics, which are generally lower than the ΛCDM predictions (for a review, see section 8 in Bernardeau et al. 2002). This poses a puzzle, because the corresponding measurements for the variance and the two-point function seem to follow the unbiased ΛCDM predictions closely on large scales.

In this paper, we present the first general results for the three-point correlation function measured from the final 2dFGRS catalogue. Preliminary measurements of three-point statistics were made using early releases of the 2dFGRS and SDSS data sets by Verde et al. (2002), Jing & Börner (2004), Wang et al. (2004) and Kayo et al. (2004). Pan & Szapudi (2005) measured the monopole moment of the three-point function in the completed 2dFGRS. Our analysis has the advantage over that of Pan & Szapudi in that it includes information about the shapes of the triangles of galaxies. A further improvement over previous approaches is a proper treatment of the correlation between data points. We follow the methodology introduced by Gaztañaga & Scoccimarro (2005, hereafter GS05) to obtain constraints on bias parameters from measurements of the reduced three-point correlation function.

This paper is organized as follows. In Section 2, we review some basic definitions involving the three-point function, as well as the methodology used for its estimation. In Section 3, we present the 2dFGRS catalogues and the associated mocks. Our results are presented in Section 4. This is quite a long section that is divided into many subsections; a detailed route map is provided at the start of this section. Our results are compared with previous analyses of the 2dFGRS in Section 5. Finally, our conclusions are presented in Section 6.

2 THEORETICAL BACKGROUND

In this section, we first give some basic definitions (Section 2.1), before discussing the expected form of the three-point correlation function (Section 2.2). We then explain how our results can be related to the predictions for the three-point function of dark matter (Section 2.3). For a comprehensive discussion of this material, we refer the reader to the review by Bernardeau et al. (2002). The method for estimating the three-point function for the 2dFGRS is set out in Section 2.4. Finally, in Section 2.5, we give an outline of how our measurement of the three-point correlation function can be used to place constraints on models of bias (for a complete discussion, see GS05).

2.1 Basic definitions: triangle shape and scale

GS05 discuss the merits of various conventions for defining triangle shapes and scales. We adopt their preferred scheme in which a triangle is defined by the ratio of the lengths of two of the sides of the triangle, $\boldsymbol{r}_{12}/\boldsymbol{r}_{23}$ and the angle between them, α:

$$\cos(\alpha) = \frac{\boldsymbol{r}_{12}}{r_{12}}\frac{\boldsymbol{r}_{23}}{r_{23}}. \quad (1)$$

The angle α can vary between 0° and 180°; for $\alpha = 0^\circ$, the third side of the triangle is given by $r_{31} = r_{12} - r_{23}$ and for $\alpha = 180^\circ$, $r_{31} = r_{12} + r_{23}$ (Fig. 1).

2.2 Three-point correlation function

The connected two- and three-point correlation functions are defined as

$$\xi(r_{12}) = \langle \delta(r_1)\delta(r_2)\rangle \quad (2)$$

$$\zeta(r_{12}, r_{23}, r_{13}) = \langle \delta(r_1)\delta(r_2)\delta(r_3)\rangle \quad (3)$$

where $\delta(r) = \rho(r)/\bar{\rho} - 1$ is the local density fluctuation around the mean $\bar{\rho} = \langle\rho\rangle$ and the expectation value is taken over different realizations of the model or physical process. In practice, the expectation value is constructed by averaging over different spatial locations in the Universe, which are assumed to form a fair sample (Peebles 1980).

The two- and three-point correlation functions change rapidly in amplitude as a function of separation. In order to study the relationship between the correlation functions in more detail, it is useful

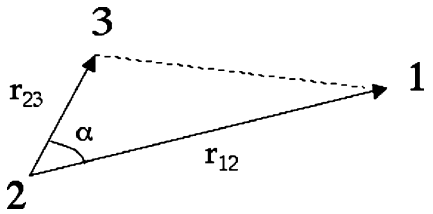

Figure 1. Three points define a triangle, which is characterized here by the two sides r_{12} and r_{23} and the interior angle α.

© 2005 The Authors. Journal compilation © 2005 RAS, MNRAS **364,** 620–634

to define the reduced three-point function, Q_3, (Groth & Peebles 1977):

$$Q_3 = \frac{\zeta(r_{12}, r_{23}, r_{13})}{\zeta_{\rm H}(r_{12}, r_{23}, r_{13})} \quad (4)$$

$$\zeta_{\rm H} \equiv \xi(r_{12})\xi(r_{23}) + \xi(r_{12})\xi(r_{13}) + \xi(r_{23})\xi(r_{13}). \quad (5)$$

Here, we have introduced a 'hierarchical' form for the three-point function, $\zeta_{\rm H}$. This quantity is built up from the products of two-point functions generated from cyclic permutations of the pair separations which make up the sides of the triangle. When Q_3 is constant, the dependence of the three-point correlation function on triangle shape and scale is fully accounted for by the corresponding changes in $\zeta_{\rm H}$; in this case, Q_3 is said to have no configuration dependence.

Previously, Q_3 was thought to be approximately constant as a function of triangle size or shape (see, for example, Groth & Peebles 1977), a phenomenon that is usually referred to as hierarchical scaling (Peebles 1980). However, GS05 showed that with sufficiently accurate theoretical predictions or for carefully constructed measurements, Q_3 is not in fact constant in any clustering regime. Nevertheless, the variation in Q_3 with scale is small when compared to the corresponding changes in ξ or $\zeta_{\rm H}$. On small scales ($<10\,h^{-1}$ Mpc), and for galaxies in redshift space (i.e. as measured by galaxy redshift surveys), GS05 showed that $Q_3(\alpha)$ displays a characteristic U-shape anisotropy moving from collapsed or elongated ($\alpha \sim 0^\circ, 180^\circ$) to more open ($\alpha \sim 90^\circ$) triangles. This effect is driven by the velocity dispersion of galaxies inside virialized structures. GS05 demonstrated that this U-shape is universal, being only very weakly dependent on scale, the primordial spectral index, or the values of the cosmological parameters. GS05 further demonstrated that this feature should be detectable in current galaxy surveys, even if the measurements are affected by shot-noise or if galaxies are biased tracers of the mass. On larger scales, the impact of velocity dispersion on the form of Q_3 is reduced, with the consequence that the U-shape tends towards more of a V-shape and approaches the (real space) perturbation theory prediction (see fig. 2 in GS05).

2.3 Theoretical interpretation

In order to interpret our measurements of Q_3 for galaxies, we compare them with theoretical predictions for dark matter in a ΛCDM universe. We first explain the form expected for the three-point function of dark matter (Section 2.3.1), before introducing a notation to quantify the differences found between galaxy and dark matter Q_3 measurements (Section 2.3.2).

2.3.1 Three-point function of dark matter

We denote the value of Q_3 for the dark matter by $Q_3^{\rm DM}$. The theoretical predictions for $Q_3^{\rm DM}$ are relatively insensitive to the precise values of the cosmological parameters, but have a strong dependence on the local spectral index, n, of the linear perturbation theory power spectrum, $P(k)$, where $n = {\rm d}\log P/{\rm d}\log k$ (see, for example, figs 9 and 10 in Bernardeau et al. 2002). This is also the case in redshift space (see fig. 4 of GS05), but where the dependence is however weaker. On the scales of interest to the present work, a change in the local spectral index of Δn translates roughly to a change in the mean amplitude of $Q_3^{\rm DM}$ by $\Delta Q_3 \simeq \Delta S_3/3 \simeq \Delta n/3$ (see Juszkiewicz, Bouchet & Colombi 1993). As an illustration, the difference in the shape of the power spectrum between CDM models with density parameters of $\Omega_{\rm m} = 0.7$ and $\Omega_{\rm m} = 0.2$ is approximately $\Delta n \simeq 0.6$ on the scales of interest here, and so the change in $Q_3^{\rm DM}$ between these models is small, $\Delta Q_3 \simeq 0.2$ (in good agreement with fig. 4 of GS05). The relative insensitivity of $Q_3^{\rm DM}$ to changes in the CDM power spectrum is important as it strengthens any conclusions we reach about differences between the value of Q_3 measured for galaxies and the predictions for the dark matter. The current levels of uncertainty on the matter density parameter, $\Omega_{\rm m}$ and the primordial spectral index $n_{\rm s}$ are around the 10 per cent level or better, and so the predicted value of $Q_3^{\rm DM}$ is tightly constrained (e.g. Percival et al. 2002; Tegmark et al. 2004; Sanchez et al. 2005).

It is also possible to use an empirical approach to estimate $Q_3^{\rm DM}$, without appealing directly to the ΛCDM model. If we assume that the two-point function of galaxy clustering has the same shape as that of the underlying mass, then the measured correlation function or power spectrum of galaxies can be used to infer the spectral index of the dark matter. The two-point correlation function and the power spectrum of galaxy clustering have both been measured for the 2dFGRS on large scales (Percival et al. 2001; Hawkins et al. 2003; Cole et al. 2005). It turns out that the shapes of these clustering statistics are compatible with the predictions of the ΛCDM model. The uncertainties in n are small ($\Delta n < 0.1$) compared to the sampling errors in the measurements of Q_3 for the 2dFGRS (GS05). We therefore assume the concordance ΛCDM model, specified by $\Omega_{\rm m} \simeq 0.3$, $\Omega_\Lambda \simeq 0.7$ and $h \simeq 0.7$, to generate predictions for $Q_3^{\rm DM}$, and neglect the impact of any uncertainty in these parameters.

2.3.2 Comparing the three-point functions of galaxies and dark matter: the implications for bias

The Q_3 value measured for galaxies may be different from the theoretical predictions for the dark matter, $Q_3^{\rm DM}$. We adopt a particularly simple scheme to quantify any such differences:

$$Q_3 \simeq \frac{1}{B}\left(Q_3^{\rm DM} + C\right). \quad (6)$$

Two numbers specify the difference between the measured and predicted Q_3: a shift or offset, C, and a scaling, B. The simple ansatz given in equation (6) is general and can, in principle, be applied on any scale. However, the interpretation of the numbers B and C does depend upon the scale under consideration. Furthermore, we should caution that this model may not necessarily always provide a good description of the transition from the clustering of the dark matter to galaxies.

The form we have chosen is motivated by perturbation theory, which applies on scales for which the correlations are small, i.e. $\xi < 1$. Fry & Gaztañaga (1993) modelled fluctuations in the density of galaxies, $\delta_{\rm G}$, as a local, non-linear expansion of fluctuations in the mass distribution, δ:

$$\delta_{\rm G} = F[\delta] \simeq \sum_k \frac{b_k}{k!}\,\delta^k. \quad (7)$$

This formalism can be used to derive a relation between the three-point function of galaxies and mass (see Fry & Gaztañaga 1993; Frieman & Gaztañaga 1994). On the weakly non-linear scales for which this transformation is a reasonable approximation, $B \approx b_1$ and $C \approx c_2 = b_2/b_1$:

$$Q_3 \simeq \frac{1}{b_1}\left(Q_3^{\rm DM} + c_2\right). \quad (8)$$

In this case, the shift by C can be interpreted as a non-gravitational contribution to $Q_3^{\rm DM}$ and B is a simple linear bias scaling. These effects can become degenerate if Q_3 is approximately constant or when the measurement errors become large. Nevertheless, it is possible, in

principle, to compare the shape of Q_3 measured for galaxies to that predicted for the dark matter, and so constrain B and C separately. Norberg et al. (in preparation, hereafter Paper I) use the two-point correlation function to obtain a working definition of the scale marking the approximate boundary between the non-linear and weakly non-linear regimes; they propose that weakly non-linear scales ($\xi \ll 1$) correspond to pair separations of $\gtrsim 9\,h^{-1}$ Mpc, whereas the non-linear regime ($\xi > 1$) is reached when $r \lesssim 6\,h^{-1}$ Mpc.

From its definition in equation (4), Q_3 is independent of the amplitude of fluctuations on large scales. We can therefore use the value of B to constrain the amplitude of fluctuations in the dark matter. In this approach, we take the two-point correlation function measured for galaxies and divide this by B^2 to obtain an empirical two-point function estimate of the dark matter. Then, after measuring the actual shape of the two-point function of the dark matter distribution from simulations, we can constrain the rms linear variance in spheres of radius $8\,h^{-1}$ Mpc, σ_8, by equating our empirical dark matter estimate to the actual value. This method for constraining σ_8 relies upon several approximations and assumptions that we have tested successfully using N-body simulations (see Paper I for a full description of the method). Similar approaches have already been attempted using the skewness of the distribution of galaxy counts-in-cells, S_3 (Fry & Gaztañaga 1993; Gaztañaga 1994; Gaztañaga & Frieman 1994), the bispectrum (e.g. Frieman & Gaztañaga 1994; Fry 1994; Scoccimarro 1998; Verde et al. 2002) and the angular three-point function (Frieman & Gaztañaga 1999).

2.4 Estimation of the three-point function

To estimate the three-point correlation function efficiently for the 2dFGRS, we use the fast grid based algorithm introduced by Barriga & Gaztañaga (2002). GS05 presented further tests of this algorithm using a wide range of numerical simulations and mock catalogues. These authors demonstrated that special attention should be paid to the grid dimension employed in order to obtain robust estimates of the three-point function in redshift space. For practical reasons, we use a somewhat lower than ideal pixel resolution in the estimation of the three-point function from the 2dFGRS. This results in some smoothing of the U-shape in $Q_3(\alpha)$ for collapsed configurations (compare fig. 5 of GS05 with our Fig. 5). As we use the same pixelization in the analysis of the mocks and dark matter theory, this loss of resolution does not affect our conclusions, although it could result in slightly less than optimal constraints on B and C.

The final 2dFGRS catalogue contains some incompleteness, which is quantified by the spectroscopic completeness mask (Norberg et al. 2002b). The spectroscopic completeness of the final 2dFGRS is much more uniform than that of the 100-K release or the samples used in earlier clustering analyses by the 2dFGRS team (e.g. Verde et al. 2002), as shown by fig. 3 of Cole et al. (2005). We reject pixels on the sky for which the spectroscopic completeness is less than 50 per cent. We account for the remaining incompleteness by applying a weight to the galaxy cell density. Further details about the 2dFGRS catalogue are given in Section 3.1.

2.5 Constraining model parameters using Q_3

The values of Q_3 measured for different opening angles are correlated. This needs to be taken into account when using measurements of Q_3 to place constraints on model parameters, such as the values of B and C defined by equation (6). GS05 introduced an eigenmode approach to parameter fitting with Q_3, and used this to demonstrate the level of the constraints on B and C that could be expected from the 2dFGRS. GS05 estimated the covariance matrix for $Q_3(\alpha)$ using the mock 2dFGRS catalogues that we describe in Section 3.2. They then obtained the inverse of the covariance matrix using the singular value decomposition method. In this approach, eigenmodes that fall below some specified signal-to-noise (S/N) threshold are discarded. The likelihood contours in the B–C plane are specified by $\delta\,\chi^2$ computed using the eigenvectors above the S/N threshold. The S/N values that we estimate are not quite optimal, because we use a finite number of mock catalogues. Our errors are therefore conservative estimates. The S/N values indicate the significance of the measurement of Q_3 (i.e. the number of standard deviations that the signal is above the noise). However, the S/N ratio does not translate directly into the size of the likelihood contours in the B–C plane, because the degeneracy between these parameters also depends on how far the measured Q_3 deviates from a constant as a function of angle. Even in the case of an infinite S/N, B and C will be degenerate if Q_3 is independent of angle (i.e. see equation 6).

3 THE GALAXY CATALOGUES

In this section, we describe the 2dFGRS data that we use to measure Q_3 (Section 3.1), and the synthetic catalogues that are employed to perform our error analysis and make the ΛCDM predictions (Section 3.2).

3.1 The 2dFGRS data

Our starting point is the final 2dFGRS catalogue (Colless et al. 2003; a full description of the construction of the survey is given in Colless et al. 2001). The 2dFGRS consists of 221 414 unique, high-quality galaxy redshifts, with a median redshift of $z \approx 0.11$ to the nominal extinction corrected magnitude limit of $b_{\rm J} \approx 19.45$. Colour information is now available for the 2dFGRS through the addition of $r_{\rm F}$-band photometry (see Cole et al. 2005). In our analysis, we consider the two contiguous regions of the survey which lie towards the directions of the South Galactic Pole (SGP) and North Galactic Pole (NGP), covering a solid angle of approximately 1200 deg^2. The redshift completeness of the survey varies with position on the sky. Colless et al. (2001) and Norberg et al. (2002b) describe a strategy for dealing with this incompleteness in clustering studies. We restrict our attention to regions of the survey for which the spectroscopic completeness exceeds 50 per cent. We note that the typical completeness for the final survey is much higher than this (∼85 per cent).

We follow the approach adopted in several previous clustering analyses of the 2dFGRS and construct volume-limited samples from the magnitude-limited redshift catalogue (Norberg et al. 2001, 2002a; Baugh et al. 2004; Croton et al. 2004a,b). This greatly simplifies the estimation of the clustering signal, as then the only variations in number density across the galaxy sample will be due to the presence of large-scale structure. A volume-limited sample is defined by an interval in absolute magnitude, and this translates into a minimum and maximum redshift. For each galaxy an absolute magnitude is computed using its redshift and apparent magnitude, and assuming the band-shift and evolutionary correction ($k + e$) advocated by Norberg et al. (2002b) (see also Cole et al. 2005). In a volume-limited sample, each galaxy could in principle be displaced to any depth within the sample and would still remain within the apparent magnitude range of the survey. In this paper we consider the samples listed in Table 1, which correspond to samples 1–4 as listed in table 1 of Croton et al. (2004b). As in Cole et al. (2005),

© 2005 The Authors. Journal compilation © 2005 RAS, MNRAS **364,** 620–634

Table 1. Properties of the combined 2dFGRS SGP and NGP volume-limited catalogues (VLCs). Columns 1 and 2 give the faint and bright absolute magnitudes that define the sample. Columns 3 and 4 give the number of galaxies in each sample and the mean number density. Columns 5 and 6 state the minimum and maximum comoving distances that bound each sample for the nominal apparent magnitude limits of the survey. All distances are comoving and are calculated assuming standard values for the cosmological parameters ($\Omega_0 = 0.3$ and $\Omega_\Lambda = 0.7$).

Magnitude range $M_{b_J} - 5\log_{10} h$		N_G	ρ_{ave} $10^{-3}/h^{-3}$ Mpc^3	D_{min} h^{-1} Mpc	D_{max} h^{-1} Mpc
−17.0	−18.0	8038	10.9	24.8	169.9
−18.0	−19.0	23290	9.26	39.0	255.6
−19.0	−20.0	44931	5.64	61.1	375.6
−20.0	−21.0	33997	1.46	95.1	537.2
−21.0	−22.0	6895	0.11	146.4	747.9

we also split the samples by rest-frame b_J–r_F colour into blue, b_J–$r_F < 1.07$, and red, b_J–$r_F > 1.07$, subsamples.

Baugh et al. (2004) and Croton et al. (2004b) both point out the impact of two superstructures, one in each of the NGP and SGP regions, on the estimation of the moments of the distribution of counts-in-cells from the 2dFGRS. The SGP structure is at $\alpha \sim 13$ h and $d \simeq 240\,h^{-1}$ Mpc and the NGP structure is at $\alpha \sim 0.5$ h and $d \simeq 325\,h^{-1}$ Mpc (see fig. 1 of Baugh et al. 2004). They found these overdensities were particularly influential on measurements made from the $L_\star$ volume-limited sample, i.e. for galaxies with $-20 < M_{b_J} - 5\log_{10} h < -19$; fainter volume-limited samples do not extend to the distance of the superstructures and brighter samples cover a larger volume and thus dilute the contribution of the structures. In this paper, we follow the approach of these authors and in Section 4.4 present measurements of the three-point function made when masking out the regions containing these superstructures. It turns out that this exclusion removes only a small fraction of the total $L_\star$ volume, approximately 2 per cent, along with the fewer than 5 per cent of the total galaxies contained within it. This exercise is merely intended to be illustrative. We are not proposing that the removal of these structures should be thought of as a correction to our measurements, but rather should serve as an indication of the magnitude of systematic effects in the estimation of higher-order statistics from surveys of the size of the 2dFGRS.

3.2 Mock catalogues

Mock catalogues play an important role in our analysis. They are used to compute errors on our measurements and also as a means of generating the predictions of the ΛCDM model, taking into account the selection function of the 2dFGRS. Following GS05, we construct the (normalized) covariance matrix for the measurements of the three-point function using an ensemble of 22 synthetic 2dFGRS catalogues extracted from the ΛCDM Hubble volume N-body simulation (Evrard et al. 2002). The construction of these catalogues is described by Norberg et al. (2002b). The mock catalogues have the same radial and angular selection function as the 2dFGRS, and have been convolved with the completeness mask of the survey. A simple phenomenological prescription has been applied to the final density field in the simulation in order to extract points with a clustering amplitude that is a modulated version of the clustering of the underlying dark matter (Cole et al. 1998). We also use the dark matter from the Hubble volume simulation to generate dark matter predictions for the concordance ΛCDM model in redshift space.

The mocks were not constructed to match higher-order clustering statistics, as the biasing model used (see Norberg et al. 2002b; Cole et al. 2005) was tuned only to reproduce the two-point correlation function of all galaxies (as measured for the 2dFGRS by Hawkins et al. 2003). In particular, this means that the mock galaxy catalogues do not display luminosity-dependent clustering, as seen in the data (Norberg et al. 2001). This deficiency can be turned around to provide an interesting test of our analysis, because the mocks should always give, for a fixed triangle configuration, the same mean $Q_3(\alpha)$ for different luminosities, regardless of the volume under consideration or the density of galaxies.

4 RESULTS FOR Q_3

In this section we present our measurements of Q_3 for different 2dFGRS galaxy samples, defined by luminosity and colour. In the first two subsections, we consider general triangle shapes, focusing first on scales for which we expect the clustering to be in the weakly non-linear regime (Section 4.1) before considering the non-linear regime (Section 4.2). The reason behind this split is that the interpretation of our measurements is quite different in these two cases, as discussed in Section 2.3. In both sections, we consider how our measurements depend upon galaxy luminosity and, in the case of the non-linear regime, on colour as well. In Section 4.3, we consider the special case of equilateral and elongated triangles, which give a cleaner measure of the physical scale dependence of Q_3. Finally, in Section 4.4, we discuss the influence of large structures on the measurement of the three-point function in the 2dFGRS. From now on, we use the shorthand notation $M^h_{b_J}$ to denote $M_{b_J} - 5\log_{10} h$.

4.1 $Q_3(\alpha)$ in the weakly non-linear regime

The $-21 < M^h_{b_J} < -20$ volume-limited subsample yields the highest S/N measurements of Q_3 in the weakly non-linear regime. Samples brighter than this have too low a galaxy density to permit robust measurements on such scales, while fainter samples span smaller volumes, resulting in a larger sampling variance. We therefore describe the results for this sample in some detail, as this will serve to make several basic points that can be applied to other samples.

4.1.1 $Q_3(\alpha)$ for $-21 < M^h_{b_J} < -20$

In the top row of Fig. 2, we show $Q_3(\alpha)$ for galaxies with $-21 < M^h_{b_J} < -20$ and different triangle configurations: $r_{12} = 9$ and $r_{13} = 9$, 18 and $27\,h^{-1}$ Mpc, from left to right respectively. The middle panel illustrates the scatter expected in such a measurement of $Q_3(\alpha)$, obtained using the mock galaxy catalogues. Here, the prediction for the ΛCDM dark matter model is shown by the solid line while the dashed line shows a biased version of this, computed by inserting $B = 1$ and $C = -0.3$ into equation (6). In the bottom panels, we show the likelihood contours for B and C derived from fitting the observed $Q_3(\alpha)$ to the ΛCDM prediction with the theoretically motivated relation given by equation (6).

In the top panels of Fig. 2 we clearly see, for the data, the characteristic dependence of Q_3 on α, with the V-shape becoming more pronounced as larger scales are considered. Note how the variation in the shape of Q_3 with scale seen in the 2dFGRS data is mimicked by the dark matter predictions and by results for the mock catalogues.

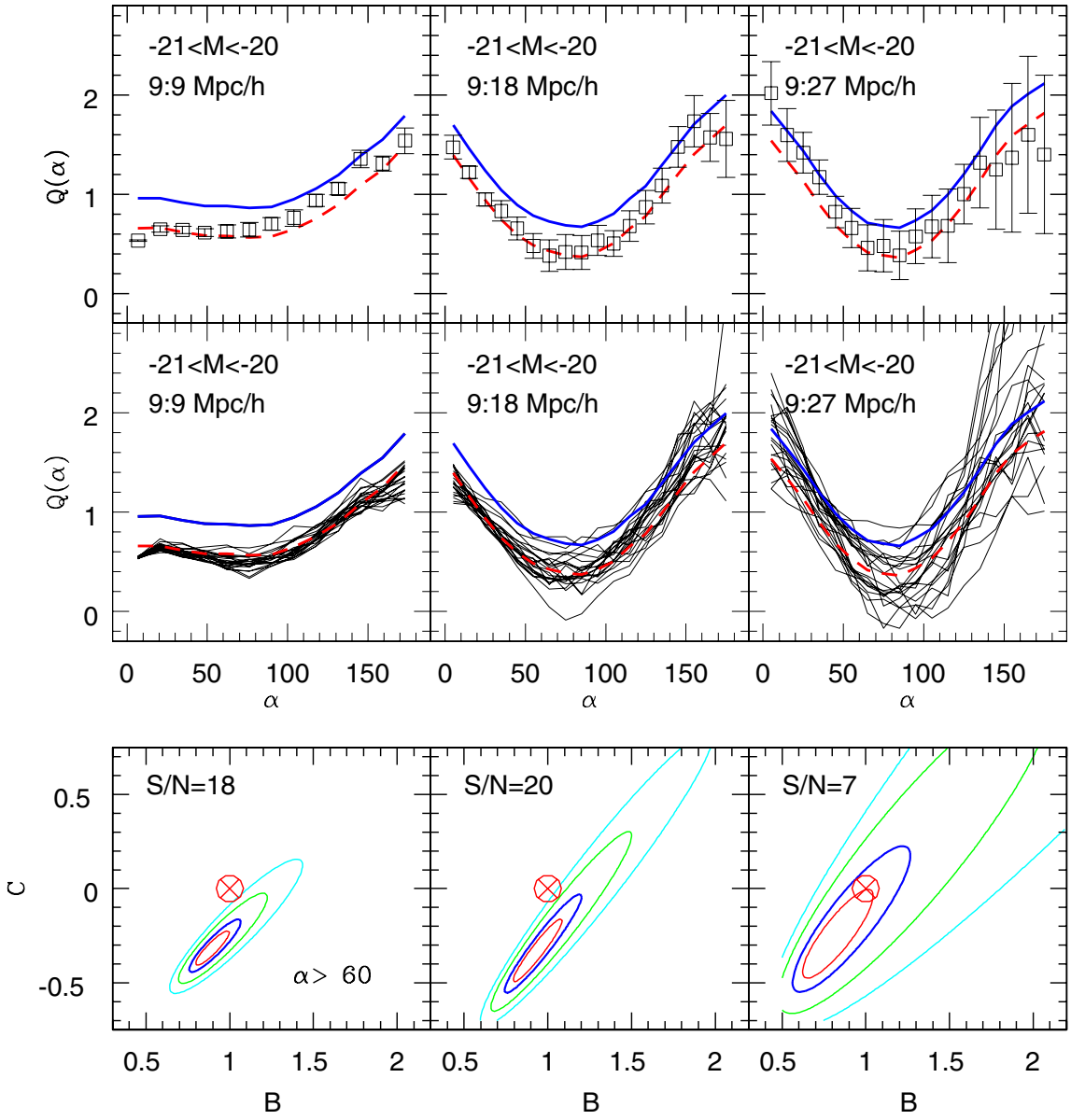

Figure 2. Q_3 in the weakly non-linear regime. The upper row shows measurements from the 2dFGRS $-21 < M^h_{b_J} < -20$ volume-limited sample. Different columns show the results for different triangle sizes, as indicated by the legend. The squares show the mean value of Q_3 as a function of α and the error bars are derived from the scatter in the mock catalogues with the same magnitude limits. The thick solid curves in the upper two rows show the predictions for Q_3 in the ΛCDM model. The thick dashed curves in these panels show the effect of applying a transformation (equation 6) to this prediction corresponding to $B = 1$ and $C = -0.3$. The thin solid lines in the middle row show the mean Q_3 measured in individual mocks. In the bottom row, we show the constraints on B and C, derived from an eigenmode analysis. The four contours shown from outside in correspond to $\chi^2 = 11$, 8, 6.17, 2.3 (i.e. 99.7, 95.4 and 68.3 per cent confidence intervals for two parameters) and $\chi^2 = 1$ (i.e. 68.3 per cent for one of the parameters). The cross point shows $B = 1$, $C = 0$ for reference.

The middle panels of Fig. 2 show how closely Q_3 estimated from the mock catalogues agrees with the measurements from the 2dFGRS. This agreement is all the more remarkable when one recalls that a match to Q_3 was not required in the construction of the mocks. Another noteworthy feature of the results for the mocks is the strong covariance that is apparent between the measurements of Q_3 in different angular bins. Hence, to perform a meaningful fit to $Q_3(\alpha)$, there is a clear need to decompose the measurement into statistically independent Q-eigenmodes, yielding a basis in which the covariance matrix is diagonal. This strong correlation between bins in measurements of $Q_3(\alpha)$ was originally pointed out by GS05. Further details of the application of the singular value decomposition to the measured values of $Q_3(\alpha)$ and the estimation of the S/N of the Q-eigenmodes can be found in GS05.

From Fig. 2, it is clear that the $-21 < M^h_{b_J} < -20$ sample provides a high-quality measurement of $Q_3(\alpha)$ in the weakly non-linear regime. The characteristic V-shape dependence of Q_3 on angle is readily apparent across a range of triangle scales. With such a high S/N of the Q-eigenmode decomposition, this volume-limited sample is expected to provide strong constraints on the parameters B and C in equation (6); we recall that in the weakly non-linear regime, $B \sim b_1$ and $C \sim c_2$. The constraints on these parameters, shown in the bottom row of Fig. 2, are discussed in Section 4.1.3

© 2005 The Authors. Journal compilation © 2005 RAS, MNRAS **364,** 620–634

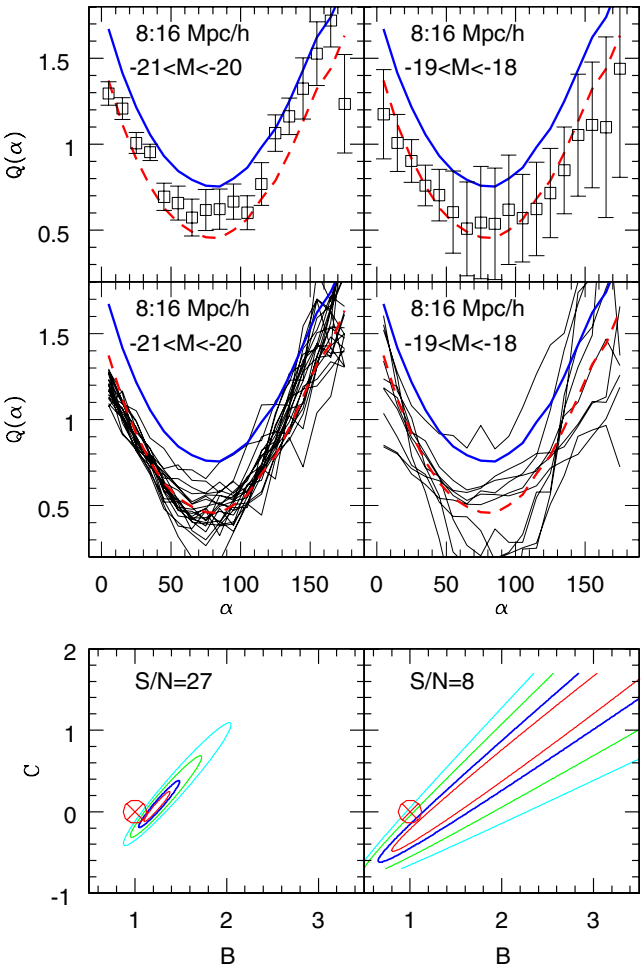

Figure 3. Same as Fig. 2, but for different volume-limited samples: $-21 < M^h_{b_J} < -20$ (left) and $-19 < M^h_{b_J} < -18$ (right). In all panels, we consider the case where $r_{23} = 2\,r_{12} = 16\,h^{-1}$ Mpc.

4.1.2 $Q_3(\alpha)$ as function of luminosity

Staying in the weakly non-linear regime, we now consider the dependence of $Q_3(\alpha)$ on galaxy luminosity. In Fig. 3 we present, for the triangle configuration $r_{13} = 2\,r_{12} = 16\,h^{-1}$ Mpc, the variation of $Q_3(\alpha)$ with luminosity, as measured from volume-limited catalogues defined by $-21 < M^h_{b_J} < -20$ and $-19 < M^h_{b_J} < -18$. On these weakly non-linear scales the best S/N, as indicated in the bottom panels of Fig. 3, again occurs for the $-21 < M^h_{b_J} < -20$ sample, as expected from the analysis of GS05.

Fig. 3 shows that the characteristic $Q_3(\alpha)$ shape is seen for both bright and faint galaxies. Moreover, the V-shape is essentially the same in the two samples, within the measurement errors. Given the size of the errors, we are not yet able to detect any clear evidence of luminosity segregation in $Q_3(\alpha)$ in the weakly non-linear regime. Unfortunately, we encounter the same limitation in Section 4.3, when considering large equilateral triangles.

From the middle panel of Fig. 3, we conclude that our measurement of Q_3 is robust to sampling variance and volume effects. Reassuringly, the results obtained from the mock catalogues for $Q_3(\alpha)$ for different volume-limited samples are, within the errors, equivalent as they should be by construction. The bottom panel of Fig. 3, which presents the constraints on B and C (equation 6), is discussed in the next section.

4.1.3 Constraints on b_1 and c_2 from $-21 < M^h_{b_J} < -20$

The bottom panels of Figs 2 and 3 present the likelihood contours for the bias model parameters B and C, as defined in equation (6), which relates $Q_3(\alpha)$ for galaxies to $Q_3^{\rm DM}(\alpha)$ for the dark matter. Remember that in the weakly non-linear regime, $B = b_1$ and $C = c_2$, the conventional linear and non-linear biasing terms, respectively. The cross-circle point in the bottom panels of Figs 2 and 3 shows an unbiased ΛCDM prediction (i.e. $b_1 = 1$ and $c_2 = 0$). For some configurations, such as the bottom-right panel of Fig. 3, the likelihood contours are broad and the bias parameters are poorly constrained. In this particular case (i.e. the faint galaxy population), this is chiefly a result of the small volume considered, telling us that these larger-scale triangle configurations do not sample enough different environments in this volume.

By combining measurements on different weakly non-linear scales, we can improve the constraints on $b_1 - c_2$ for the $-21 < M^h_{b_J} < -20$ sample, as shown in Fig. 4. Table 2 lists the corresponding marginalized best-fitting values. In this regime, we do find a slight trend, with a decrease of the bias parameters with increasing

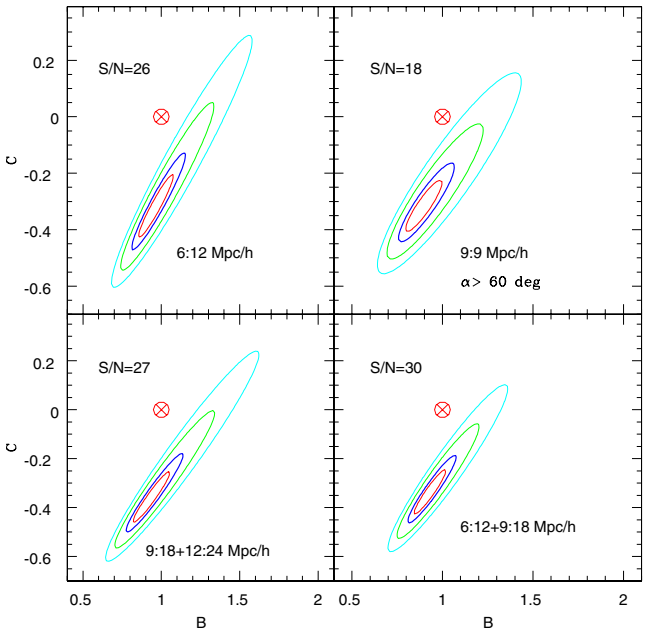

Figure 4. The combined constraints on B and C, in the weakly non-linear regime, using different triangle configurations and the joint covariance of $Q_3(\alpha)$ for the 2dFGRS volume-limited sample $-21 < M^h_{b_J} < -20$. Each panel uses different triangle configurations (as indicated by each legend). For isosceles triangles with $r_{12} = r_{23} = 9\,h^{-1}$ Mpc, we fit only for $\alpha > 60^\circ$, to ensure that only weakly non-linear scales (9–18 h^{-1} Mpc) are considered.

Table 2. The best-fitting b_1 and c_2 values for the $-21 < M^h_{b_J} < -20$ sample for a range of weakly non-linear scales, along with the associated marginalized 68 per cent confidence intervals (corresponding to 1σ if one assumes Gaussian statistics), as taken from Fig. 4. Each entry in the table uses different triangle configurations (indicated in brackets in the first column), probing the range of scales listed in the first column.

Scale (h^{-1} Mpc)	b_1	68 per cent C.I.	c_2	68 per cent C.I.
6–18 (6:12)	1.01	[0.91,1.15]	−0.27	[−0.37,−0.15]
6–27 (6:12+9:18)	0.93	[0.85,1.03]	−0.34	[−0.42,−0.23]
9–18 (9:9, $\alpha > 60^\circ$)	0.97	[0.88,1.09]	−0.31	[−0.41,−0.24]
9–36 (9:18+12:24)	0.94	[0.83,1.07]	−0.36	[−0.45,−0.23]

scale, although the trend is not very significant and is within the quoted 1σ error. The strongest constraints on $b_1 - c_2$ come from the 6–27 h^{-1} Mpc configuration (bottom-right panel in Fig. 4), with measured values of $b_1 = 0.93^{+0.10}_{-0.08}$ and $c_2 = -0.34^{+0.11}_{-0.08}$.

Finally, we note that in all the panels of Fig. 4 the unbiased ΛCDM prediction (shown by the cross-circle) is strongly excluded by the data. For example, for $r_{13} = 2\,r_{12} = 18\,h^{-1}$ Mpc, $\Delta\chi^2 > 80$ for two degrees of freedom (which implies a disagreement in excess of 9σ). Despite the correlation between b_1 and c_2, the significance of the detection of bias, i.e. values away from $b_1 = 1$ and $c_2 = 0$, is much larger than is apparent from just adding the errors in quadrature or using the values in Table 2 with a square error box. In fact, the measured values of b_1 and c_2 seem to follow a degenerate line, illustrated in Fig. 4, which avoids $b_1 = 1$ and $c_2 = 0$ for all scales and luminosities. As the scale or the luminosity of the sample decreases, b_1 crosses unity and c_2 passes through zero (although not at the same time), following $b_1 \simeq c_2 + 1.2$ and hence avoiding the unbiased prediction.

4.2 $Q_3(\alpha)$ in the non-linear regime

In this section, we consider triangle configurations which probe non-linear clustering scales corresponding to $\lesssim 6\,h^{-1}$ Mpc (see Section 2.3). We first discuss results for three different triangle configurations using the $-19 < M^h_{b_J} < -18$ volume-limited catalogue (Section 4.2.1). This is found to be the optimal sample with which to study the non-linear regime due to its relatively high galaxy number density in a volume that is large enough to account for small-scale cosmic variance. Thus, this sample is the one least affected by shot noise.[1] Then, in Section 4.2.2, we consider the variation of $Q_3(\alpha)$ with luminosity and colour on non-linear scales, followed by a study of the constraints on the model parameters B and C (equation 6) in Section 4.2.3

4.2.1 $Q_3(\alpha)$ for $-19 < M^h_{b_J} < -18$

The bottom row of Fig. 5 shows $Q_3(\alpha)$ for the $-19 < M^h_{b_J} < -18$ sample with three triangle configurations which probe non-linear scales. From left to right, we have $r_{13} = 2\,r_{12}$ with $r_{12} =$ 6, 3 and $1.5\,h^{-1}$ Mpc, respectively. For these configurations, the characteristic U-shape of $Q_3(\alpha)$ is clearly visible. The 1σ errors are found to increase on larger scales due to the reduced number of independent triangle configurations that one can fit within the sample. The S/N for these triangle configurations is 8, 22 and 18, respectively, as indicated in the bottom row of Fig. 6. Such values are not exceptional, but nevertheless are sufficient to allow useful constraints on B and C to be determined. These model constraints are further discussed in Section 4.2.3

4.2.2 $Q_3(\alpha)$ as function of luminosity and colour

We use bright ($-21 < M^h_{b_J} < -20$) and faint ($-19 < M^h_{b_J} < -18$) volume-limited samples to investigate the luminosity dependence of $Q_3(\alpha)$ in the non-linear regime. This is presented in Fig. 5 (top and bottom panels) for different triangle configurations (from left to right). In Fig. 6, we show the corresponding likelihood contours for the model parameters B and C from equation (6). Comparing the results between the faint and bright galaxy samples in Fig. 5, we see that, even though the characteristic U-shape is generally preserved, there is a weak tendency for the amplitude of $Q_3(\alpha)$ to decrease with increasing galaxy luminosity. In terms of the model parameters B and C, Fig. 6 suggests that changing the characteristic luminosity of the galaxy population results in a shift in the best-fitting model.

This general behaviour is better quantified in Fig. 7, which shows how Q_3 changes with both colour and luminosity. The red and blue colour samples are subpopulations of each volume-limited sample, split by rest-frame b_J–r_F colour at b_J–$r_F = 1.07$ (Cole et al. 2005). We focus our attention on two characteristic configurations: equilateral triangles, with $\alpha \simeq 60^\circ$, and elongated triangles with

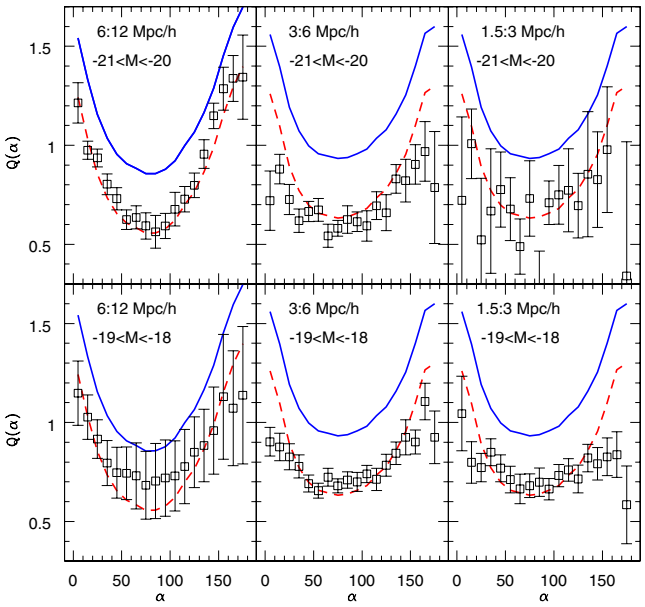

Figure 5. $Q_3(\alpha)$ in the non-linear regime for two different luminosities (increasing from bottom to top) and different scales (decreasing from left to right), as indicated in the legend in each panel. The biased model (dashed lines) has $B = 1$ and $C = -0.3$, whereas Q_3 for ΛCDM is plotted with a solid line.

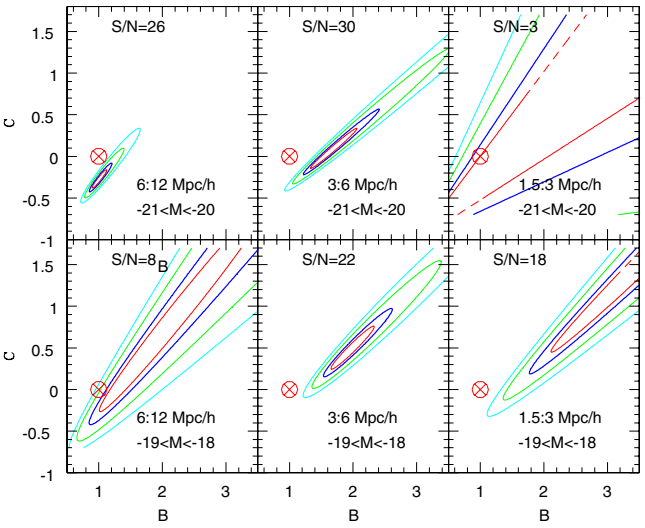

Figure 6. Constraints on the model parameters B and C, for the samples presented in Fig. 5.

[1] The $L_\star$ sample is actually statistically better than this fainter one, but suffers from a much larger systematic uncertainty due to the presence of the two superstructures (see Section 4.4).

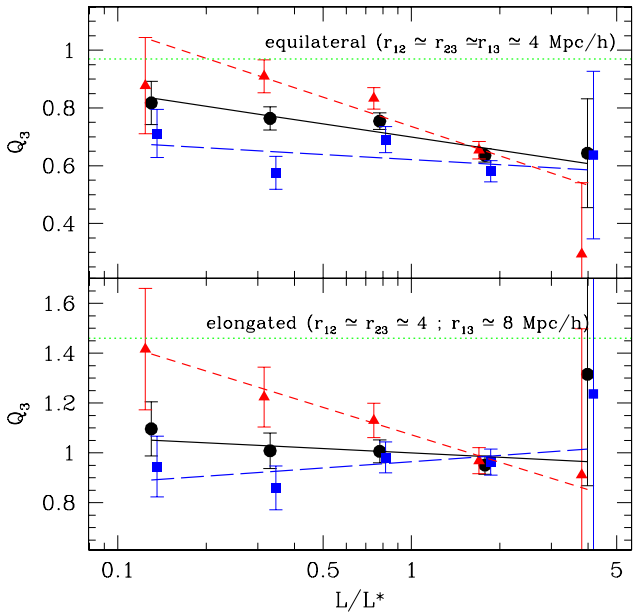

Figure 7. Values of Q_3 for equilateral (upper panel) and elongated (lower panel) triangles, as a function of luminosity. Measurements with error bars show different galaxy samples: all galaxies (circles), red galaxies (triangles) and blue galaxies (squares). The solid, short-dashed and long-dashed lines show the corresponding best linear fit to equation (9), with the best-fitting values of the parameters quoted in Table 3. The dotted horizontal line shows the corresponding ΛCDM prediction.

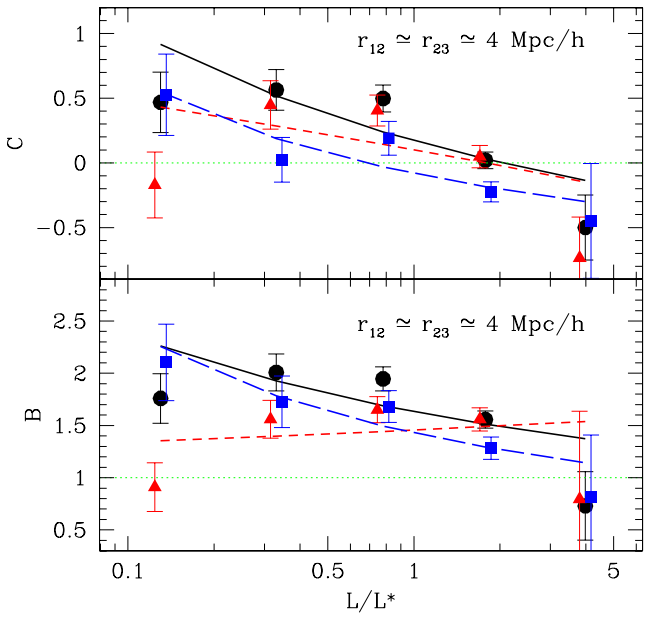

Figure 8. Deviations of Q_3 from the ΛCDM prediction as quantified by B and C (see equation 6; recall that, for the dark matter, $B = 1$ and $C = 0$, as shown by the horizontal dotted line in each panel). Results are shown for all configurations of triangles with $r_{12} \simeq r_{23} \simeq 4\,h^{-1}$ Mpc, as a function of luminosity. Circles, triangles and squares with error bars correspond to all, red and blue galaxies, respectively. Continuous, short-dashed and long-dashed lines show the corresponding predictions for all, red and blue galaxies using the best-fitting parameters listed in Table 3 and equation (9).

Table 3. The best-fitting Q_3^* and slope α_L of equation (9) for different configurations (equilateral and elongated), for different galaxy populations (all, red and blue) and dark matter (DM).

Triangle	Sample	Q_3^*	α_L	χ^2
Equilateral	All	0.70 ± 0.02	-0.15 ± 0.04	3.1
Equilateral	Red	0.74 ± 0.04	-0.34 ± 0.11	4.2
Equilateral	Blue	0.62 ± 0.03	-0.06 ± 0.07	4.3
Equilateral	DM	0.97 ± 0.03	0	
Elongated	All	0.99 ± 0.04	-0.06 ± 0.09	1.7
Elongated	Red	1.07 ± 0.02	-0.37 ± 0.03	0.2
Elongated	Blue	0.96 ± 0.03	0.08 ± 0.08	1.2
Elongated	DM	1.46 ± 0.03	0	

$\alpha \simeq 180°$. We choose a common scale around $r_{12} \simeq r_{23} \simeq 4\,h^{-1}$ Mpc, where all samples yield a good detection of Q_3. To improve the S/N, we take a large α bin, $\Delta\alpha = \pm 18°$, and a large r_{12} bin, $\Delta r_{12} = \pm 1\,h^{-1}$ Mpc, compared to our standard choices of $\Delta\alpha = \pm 5°$ and $\Delta r_{12} = \pm 0.6\,h^{-1}$ Mpc.

The results in Fig. 7 are well fit by a linear relation that is a function of absolute magnitude:

$$Q_3 = Q_3^* + \alpha_L \log_{10} \frac{L}{L^*} = Q_3^* - 0.4\,\alpha_L\,(M - M^*). \qquad (9)$$

Table 3 shows the best-fitting values for the parameters Q_3^* and α_L using a χ^2 fit with the full covariance matrix. As shown by the χ^2 values in the table, the functional form given in equation (9) provides a very good description of these measurements. As seen in Table 3 and also in Fig. 7, there is weak evidence for luminosity segregation in both the blue and red populations. Interestingly, the small but significant trend for the overall population can be fully attributed to the luminosity segregation in the red galaxies.

4.2.3 Constraints on B and C from non-linear scales

Fig. 8 shows, as symbols with error bars, the best-fitting values for B and C (see equation 6) in the non-linear regime using all isosceles triangle configurations with $r_{12} \simeq r_{23} \simeq 4\,h^{-1}$ Mpc, i.e. not just the elongated and equilateral cases considered in Fig. 7. We find weak systematic trends in the values of these parameters with luminosity, with fainter galaxies favouring larger values of B and C. All samples, except the brightest, are at least 1σ or 2σ away from the unbiased ΛCDM case (i.e. $B = 1$ and $C = 0$). Fig. 8 also indicates, using lines, the corresponding values of B and C when we use the best linear fit to the Q_3 data as a function of luminosity, as listed in Table 3. These lines emphasize the monotonic behaviour of the data and provide some additional idea of the uncertainties.

We note that if the naive interpretation of B is taken as the linear bias parameter, b_1, then the behaviour shown in Fig. 8 is exactly the opposite to that previously reported from the analysis of the two-point correlation function, ξ_2, over similar volume-limited samples (Norberg et al. 2001, 2002a; Paper I). However, in our case here, the measurement of the parameter B is carried out in the non-linear clustering regime, where B can no longer be interpreted as the linear bias parameter. This is why our notation explicitly differentiates between B and b_1, and explains our choice to split the analysis into the two distinct clustering regimes. On small scales, we expect strong corrections to the linear relation $\xi_2 \simeq b_1^2 \xi_2^{\rm DM}$ and similarly to equation (6). Indeed, the expansion used in equation (7) is only valid in regimes where the density fluctuations are small with $\delta < 1$. Thus, the fact that B, as measured from $Q_3(\alpha)$, decreases with increasing luminosity does not necessarily mean that $\xi_2/\xi_2^{\rm DM}$ should decrease for brighter galaxies. Once we are in the non-linear regime, B and C can only be understood in terms of their effect on $Q_3(\alpha)$, i.e. a shift

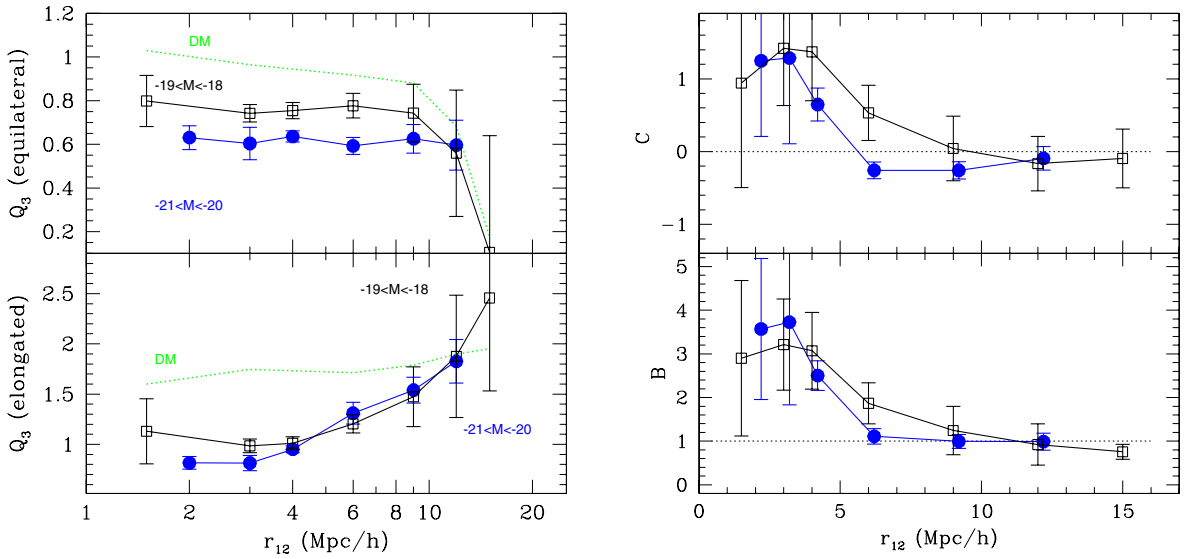

Figure 9. Left panels: the upper and lower panels show, as a function of the triangle side length, Q_3 for equilateral and elongated configurations, respectively. Squares and dots correspond to the $-19 < M^h_{b_J} < -18$ and $-21 < M^h_{b_J} < -20$ galaxy samples, respectively. For equilateral triangles, we detect a clear luminosity segregation on non-linear scales and no significant scale dependence for galaxies of a given luminosity. This is in contrast to elongated triangles, where a strong scale dependence is observed but with no indication of luminosity segregation on any scale. The dotted lines in each panel show the ΛCDM prediction for $Q_3(r_{12})$. Right panels: best-fitting B and C values for the combined configurations shown in the left panel, for the $-21 < M^h_{b_J} < -20$ (dots) and $-19 < M^h_{b_J} < -18$ (squares) samples. Note the change to a linear scale in the x-axis.

and scale modification of the $Q_3^{\rm DM}(\alpha)$ dark matter configuration, and not in terms of the theoretically motivated relation given by equation (7). Even with these interpretative restrictions, the values of B and C that we recover provide an accurate description of how biasing changes $Q_3^{\rm DM}(\alpha)$ and so give interesting new constraints on models of galaxy formation.

4.3 Q_3 as a function of scale

We present in Fig. 9 results for Q_3 using equilateral and elongated triangle configurations for the $-19 < M^h_{b_J} < -18$ and $-21 < M^h_{b_J} < -20$ volume-limited samples. These two configurations correspond to isosceles triangles with $\alpha = 60^\circ$ and $\alpha = 180^\circ$, respectively. The equilateral configuration has the nice property that it can be fully characterized by just one triangle side length, so that each triangle samples a unique scale. Fig. 9 shows that for the equilateral configuration (upper panel), Q_3 displays little scale dependence, as opposed to the elongated case (lower panel), which shows a rather strong scale dependence, much stronger than the dark matter prediction for similar triangle configurations. In addition, on non-linear scales, the equilateral configuration also provides clear evidence for luminosity segregation, although on weakly non-linear scales the results are currently too uncertain to continue making such a claim. This, unfortunately, mirrors our conclusions from Section 4.1.2, using other triangle configurations. Elongated measurements of Q_3, in contrast, display no luminosity dependence at all.

From Fig. 9, we conclude that both triangle configurations, when probing weakly non-linear scales, are in reasonably good agreement with the ΛCDM prediction, favouring nevertheless a slightly negative value for C. This is in good agreement with the results presented in Table 2. On non-linear scales, the difference between the data and the dark matter prediction is striking and will provide a powerful constraint on models of galaxy formation. Note that the results presented in Fig. 9 are fully consistent with those discussed in Section 4.1.3 The aim of the exercise of considering isosceles triangles is to isolate the dependence of Q_3 on scale. To achieve this, the binning of Q_3 as a function of α is degraded and the range of values of α considered on weakly non-linear scales is reduced when compared with the earlier, less restrictive analysis in Section 4.1.3 (which considered also triangles with $r_{13} > r_{12}$ and better α resolution). As a consequence, the resulting constraints on the parameters B and C presented in this subsection have larger error bars.

4.4 Influence of superstructures on Q_3

The measured Q_3 for the $L_\star$ sample, i.e. galaxies with absolute magnitudes in the range $-20 < M^h_{b_J} < -19$, can be strongly influenced by the presence of two superstructures in the 2dFGRS, depending on the scale measured. The impact of these structures on the distribution of counts-in-cells in the $L_\star$ sample was first pointed out by Baugh et al. (2004). They presented results both with and without the superstructures, to illustrate the systematic effect that their presence has upon the clustering measurements. For the $L_\star$ sample, the superstructures were found to dominate the clustering statistics on scales larger than $\approx 6\,h^{-1}$ Mpc, and we find that these structures have a comparable influence in our analysis, as shown in Fig. 10 (in general, the influence of these structures can be seen out to the largest scales that can be probed). On smaller scales ($r_{13} < 6\,h^{-1}$ Mpc), and for the other volume-limited samples that we consider, either the systematic contribution from these large coherent structures lies within the (correlated) error bars from the mocks, or, because of their spatial location, the superstructures are not present within the volume analysed.

The impact of the superstructures is equally pronounced in both the NGP and SGP regions, as is clear from the left panel of Fig. 10. Both the NGP and SGP results for $Q_3(\alpha)$ (solid and dashed lines, respectively) change in a similar way when the superstructure in each region is removed. As we pointed out in Section 3, the volume masked out when the superstructures are excised is less than 2 per cent of the total, with a loss of approximately 5 per cent of

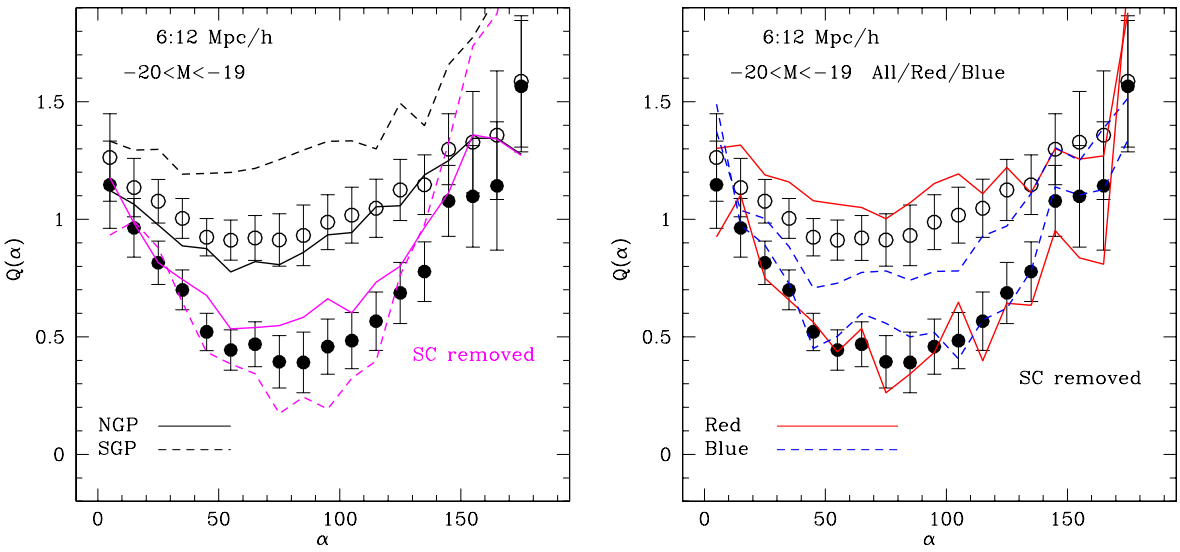

Figure 10. The impact of the superstructures on the measurement of $Q_3(\alpha)$ for the $-20 < M^h_{b_J} < -19$ sample and the $r_{23} = 2\,r_{12} = 12\,h^{-1}$ Mpc triangle configuration. Open and filled circles show respectively the results with and without the superstructures (SC). All error bars are derived from the mocks and correspond to a 2σ limit. Left panel: solid (dashed) lines show results for the NGP (SGP) region. The upper pair of lines and set of symbols show the results with the SC; the lower set without SC. Right panel: solid (dashed) lines correspond to blue (red) galaxies. As in the left panel, the upper pair of lines and set of symbols show the results with the SC; the lower set without SC.

the galaxies. As Baugh et al. remarked, the act of removing the superstructures is not intended to serve as a correction to the clustering measurements, but rather as an illustration of the systematic effects that rare objects produce in higher-order clustering statistics. That said, the results with the superclusters removed do appear to be more in line with our theoretical prejudice for the weakly non-linear regime.

The difference between the results obtained for $Q_3(\alpha)$ with and without the superstructures is larger than the variance over our ensemble of 22 mock catalogues. This indicates that the volume-limited samples in the 22 mocks do not contain the large, coherent structures seen in the real data, as mentioned above. As Baugh et al. (2004) commented, the presence of such structures could give us new insights into models of structure formation. However, it is important to bear in mind that the lack of superstructures in such a small number of mocks does not place a very high confidence limit against them being seen at all in the ΛCDM model. All that we can conclude from the non-detection of such objects in our ensemble of synthetic 2dFGRS catalogues is that they occur less than 5 per cent of the time. We have carried out an analysis of a large ensemble of dark matter simulations, in addition to undertaking a more extensive search of the Hubble volume simulation, in order to place tighter constraints on the frequency of such superstructures in the ΛCDM cosmology. Before we can place firm limits on the chances of finding superstructures like those seen in the 2dFGRS, we need to make realistic mocks with the radial and angular selection of the 2dFGRS, but the preliminary indication from analyzing idealized, cubical volumes is that it is possible to find such superstructures in the simulations. Full details will be presented in a future paper (see also Fosalba, Pan & Szapudi 2005, who discuss the impact 10^{15} solar masses haloes on the theoretical prediction of Q_3).

In the right panel of Fig. 10, we show, for the same triangle configuration as in the left panel, the results for $Q_3(\alpha)$ split by colour: red (solid) and blue (dashed). It is interesting to see that with the superstructures included, the difference between Q_3 measured for red and blue galaxies is mildly significant (with red galaxies having a systematically larger Q_3). In contrast, when the superclusters are excluded from the analysis, the measured Q_3 for red and blue galaxies are identical to within the errors. This segregation suggests that the superstructures are, perhaps not unsurprisingly, populated preferentially by red galaxies.

5 COMPARISON WITH PREVIOUS 2dFGRS RESULTS

As mentioned in the introduction, Baugh et al. (2004) and Croton et al. (2004b) found the puzzling result that $S_3 \simeq 2$ for 2dFGRS galaxies in contrast to the theoretical value of $S_3^{\rm DM} \simeq 3$ expected in ΛCDM on large (weakly non-linear) scales. This apparent inconsistency can now be resolved using the bias parameters we have measured here, i.e. $b_1 \simeq 1$ and $c_2 \simeq -0.3$ gives $S_3^G \simeq (S_3^{\rm DM} + 3c_2)/b_1 \simeq 2$, in good agreement with the above measurements on large scales. In their fig. 10, Croton et al. (2004b) found a weak dependence of S_3 on galaxy luminosity, with a slope $B_3 \simeq -0.4$ detected with 2σ confidence level. We note that this is in very good agreement with our nearly 4σ detection of $\alpha_L \simeq -0.15 \pm 0.04$, as quoted in Table 3. Because $S_3 \simeq 3\ Q_3$, we would expect $B_3 \simeq 3\ \alpha_L \simeq -0.45 \pm 0.12$, as found in Croton et al. (2004b), but with a higher significance.

Measurements of three-point statistics from early 2dFGRS data releases were made by Verde et al. (2002) and Jing & Börner (2004). These authors used compilations comprising 127-K and 100-K galaxies, respectively. Here, as remarked earlier, we use the final data set which contains double the number of galaxies and double the volume that were available for analysis in these preliminary studies. Recently, Pan & Szapudi (2005) have also analysed the final 2dFGRS data set, estimating the monopole moment of the three-point function, averaging over the shape dependence of triangles. In this section, we compare our results with those obtained by these authors and also with the measurement of the projected Q_3 for the Automated Plate Measurement (APM) survey, the parent catalogue of the 2dFGRS, made by Frieman & Gaztañaga (1999).

Verde et al. (2002) found, using a three-point function analysis in Fourier space, that 2dFGRS galaxies are essentially unbiased tracers of the mass, recovering a linear bias factor consistent with unity, $b_1 = 1.04 \pm 0.11$, and a second-order bias that is effectively zero, $b_2 \equiv b_1 c_2 = -0.054 \pm 0.08$. We note that Lahav et al. (2002) also reached a similar conclusion applying a different approach to the same 2dFGRS data set, arguing that $b_1 \sim 1$. There is good agreement between our best value for b_1 and that obtained by Verde et al., which is encouraging in view of the possible reasons for discrepancies between the results of the two studies set out below. However, our results for the quadratic bias are quite different from those of Verde et al. Our optimum measurement gives a 3σ detection of a non-zero value for the quadratic bias, whereas Verde et al. found a value consistent with zero. The discrepancy between our results and those of Verde et al. corresponds to $\Delta\chi^2 > 80$ for two degrees of freedom. This implies a 9σ discrepancy (recalling that the error boxes are not square, but elongated). The discrepancy in the claimed values of c_2 is only 3σ–4σ if we take the nominal errors on the measurement of c_2 by Verde et al. and assume square error boxes.

What are the reasons behind this disagreement? We have identified some aspects in which our analysis differs from that of Verde et al., which will contribute to the discrepancy at different levels, over and above the fact that we used different versions of the 2dFGRS data. First, we have considered the full 2dFGRS in configuration space, thus avoiding the need to compensate for the impact of the complicated 2dFGRS angular mask on measurements carried out in Fourier space. Verde et al. do not correct for the convolution of the underlying bispectrum with the angular survey window function, arguing that, for the range of wavenumbers they consider, this effect is unimportant. This conclusion is based upon tests carried out for the power spectrum by Percival et al. (2001). The impact of the window function on the bispectrum could be more extensive than in the case of the power spectrum, introducing anisotropies into the recovered bispectrum, and has not been tested explicitly. Secondly, the range of galaxy luminosities considered is different in the two studies. We have analysed volume-limited samples drawn from the 2dFGRS, whereas Verde et al. used the flux-limited survey (however, our best measurement comes from galaxies with luminosities between 1.3 and 2.5 $L_\star$, and their sample corresponds to $\sim$1.9 $L_\star$). Thirdly, the scales used to constrain the parameters of the bias model are also different. We use triangles that probe pair separations from 9 to $36\,h^{-1}$ Mpc; Verde et al. consider 13–$62\,h^{-1}$ Mpc, although most of their signal comes from the smaller scales, as shown by their fig. 4. Fourthly, Verde et al. neglect the covariance between measurements of the bispectrum at different wavenumbers, which is a poor approximation even in Fourier space, as shown by Scoccimarro et al. (2001a) and Feldman et al. (2001). Neglecting the covariance will artificially suppress the errors on b_1 and b_2 by a considerable factor, corresponding roughly to the actual number of bins used divided by the number of dominant eigenmodes of the reduced three-point function, which in this case could be up to a factor of 4. This could to some extent explain why our relative errors are larger than those quoted by Verde et al., in spite of the more homogeneous 2dFGRS data set used in our analysis. Verde et al. use mock catalogues to estimate the errors on the recovered values of b_1 and b_2. The true, underlying value of b_2 for the mocks is not known, so it is not possible to assess whether or not their method introduces any systematic biases in the recovered value of b_2. A bias on b_2 introduced by the convolution with the angular mask and the covariance in the bispectrum measurements could affect the estimated values of both the mean and the errors. In fact, the mocks used by Verde et al. are very similar to those used here as they were produced using the same prescription for galaxy biasing. As shown by the dashed lines in our Figs 2, 3 and 5 there is a systematic shift of Q_3 in the mocks with respect to the dark matter simulations, indicating that b_2 is in fact non-zero (and negative) in the mocks, in contrast to fig. 2 of Verde et al.

Our results are in somewhat better agreement with those of Jing & Börner (2004) and Wang et al. (2004), who analysed the 2dFGRS 100-k release (Colless et al. 2001). They found that Q_3 measured for the 2dFGRS is smaller than the ΛCDM predictions, particularly for galaxies brighter than $L_\star$. This agrees with our result (compare the measurements for galaxies shown by symbols in the top rows of Figs 2 and 3 with the dark matter predictions plotted using thick lines) and is also at odds with the Verde et al. result. Our results for equilateral configurations in Fig. 7 are also in good agreement with fig. 10 in Wang et al. (2004). However, the comparison with these results is not straightforward for a number of reasons. (i) The authors used less than half the data that we have analysed. (ii) They used a different parametrization and binning for their measurements of Q_3. (iii) They neglected covariance between bins and used approximate bootstrap errors. Jing & Börner interpreted the lower values of Q_3 that they found as a consequence of a larger linear bias, $b_1 \simeq 1.5$, in contrast to our conclusion that most of the bias comes from the quadratic term $c_2 \simeq -0.3$, with a linear bias consistent with unity. This difference has a dramatic consequence for the implied value of σ_8. For galaxies fainter than $L_\star$, Jing & Börner obtain unbiased results, which disagrees with our findings. This, however, could be a result of the smaller volume probed by Jing & Börner, which gives larger errors on their measurement. Jing & Börner also seem to find less configuration dependence for Q_3, i.e. as a function of the triangle shape specified by α. As pointed out in GS05, this could partly be due to the use of too large a bin in the α angle that parametrizes triangular shape in addition to the smaller volume used.

Most recently, as this paper was about to be submitted, Pan & Szapudi (2005) presented new results on the monopole moment of the three-point function measured from the full 2dFGRS. They find $b_1 \simeq 1.04^{+0.23}_{-0.09}$ and $b_2 \simeq -0.06^{+0.03}_{-0.01}$. Both the technique and assumptions employed by Pan & Szapudi are conceptually very different from ours. The monopole contribution to the normalized three-point function merely yields a constant value that is independent of triangle opening angle. It is approximately equivalent to the first eigenmode in our singular value decomposition of the covariance matrix of Q_3, and therefore contains much less information than we use to place constraints on the bias parameters. As a consequence, the monopole alone cannot be used to separate b_1 from b_2; only the higher multipoles of Q_3 can break this degeneracy. Pan & Szapudi instead use a simultaneous fit to the amplitudes of the two (ξ) and three-point (ζ) functions (as a function of scale) to place separate constraints on the values of b_1 and b_2; recall that our analysis only requires a fit to the ratio $Q_3 \sim \zeta/\xi^2$. Both the modelling and the systematics involved in the fit used by Pan & Szapudi are therefore quite different from ours. Our analysis is less sensitive to possible systematics in the amplitude of ζ. In particular, we do not need to model the impact of redshift distortions on the amplitudes of the two- and three-point functions as Pan & Szapudi must. Another important difference is the implicit assumption used by Pan & Szapudi that the biasing parameters, b_i, are constant over the whole range of scales considered, i.e. from $4 - 60\,h^{-1}$ Mpc. In our case, we allow b_i to change for each combination of fixed scales r_{12} and r_{23}. Given these differences, there is surprisingly good agreement in the values obtained for b_1 by the two methods. However, their b_2 value is significantly different. This is not unexpected given the systematic uncertainties in modelling redshift distortions through the f_2^2 term

in equation (6) of their paper. As shown in the right-hand panel of our Fig. 9 and in Table 2, we find a weak trend for the bias parameters to increase as the triangle scale is reduced. This could also help to explain the slightly larger biasing parameters they find. Perhaps more puzzling is their fig. 7, which shows how b_1 increases for the brightest galaxies, in contrast to our Fig. 7 (which only applies to the smallest scales considered by Pan & Szapudi).

Our findings are compatible with the values of the projected Q_3 measured in the APM survey, which is the parent catalogue of the 2dFGRS. Frieman & Gaztañaga (1999) also found values of Q_3 that lay below the ΛCDM predictions. However, they did not perform a proper S/N analysis with the covariance matrix to separate b_1 from b_2.[2] Our results are also in qualitative agreement with the values of the angular skewness, s_3, measured in the APM galaxy survey (Gaztañaga 1994). The mean over large angular scale (corresponding to $7 - 30\,h^{-1}$ Mpc) was estimated to be $s_3 = 3.8$, with an error (dominated by sampling covariance) of the order of $\gtrsim$10 per cent. The theoretical predictions for the projected moments using perturbation theory (Bernardeau 1995) and dark matter simulations (Gaztañaga & Bernardeau 1998) yield a mean value $s_3 \simeq 5$ over the same scales.[3] The skewness measured from the APM survey is thus also below the ΛCDM prediction. This agrees well with our estimates of the bias parameters $b_1 \simeq 1$ and $c_2 \simeq -0.3$, which give $s_3^G \simeq (s_3 + 3c_2)/b_1 \simeq 4$, in excellent agreement with the observed APM values. Note that the APM results correspond to configuration space, in contrast to our results which are in redshift space. Thus, our simple quadratic bias model (in redshift space) can account simultaneously for observations of real-space (projected) and redshift-space results for three-point statistics (both skewness and three-point function). Our new result solves the long-standing observational puzzle regarding how the measured and predicted values of S_3 and Q_3 can be reconciled.

6 CONCLUSIONS

We have measured the reduced three-point function $Q_3(r_1, r_2, r_3) \sim \zeta/\xi^2$ (as defined in equation 5>) in the final 2dFGRS catalogue, using triangles of different scales and opening angles. We have utilized a range of volume-limited samples in our analysis, which allows us to look for clustering trends as a function of galaxy luminosity. The inclusion of r_F-band photometry in the final 2dFGRS data release also allows us to look for a dependence of the three-point function on galaxy colour. Another novel aspect of our analysis is that we employ an eigenmode decomposition to deal with correlations between data points and to assess the S/N of our measurements; our results typically have a S/N >20.

There are two primary motivations for measuring the reduced three-point function. The first is to test the gravitational instability paradigm for the formation of large-scale structure in the Universe. There are clear predictions for the form of the three-point function in the case of an initially Gaussian distribution of density fluctuations that have evolved under gravity (see Bernardeau et al. 2002). The second motivation is to provide new constraints on models of galaxy formation, by establishing how the three-point function of galaxies differs from that of the underlying dark matter. It turns out that the predictions for the dark matter are insensitive to the amplitude of density fluctuations and to the detailed shape of the power spectrum.

We have divided our analysis into two clustering regimes: weakly non-linear clustering (i.e. $r \gtrsim 6\,h^{-1}$ Mpc or $\xi \lesssim 1$) and non-linear clustering ($r \lesssim 6\,h^{-1}$ Mpc or $\xi \gtrsim 1$). On weakly non-linear scales, there is a striking similarity between the shape of Q_3 measured for galaxies and the predictions for the dark matter. This supports the idea that the basic phenomenon behind the clustering pattern of galaxies is gravitational instability, which confirms our previous conclusions reached from the analysis of the distribution of counts-in-cells for the 2dFGRS (Baugh et al. 2004; Croton et al. 2004b).

There are, however, significant differences, between Q_3 measured for galaxies and the expectations for a ΛCDM universe. We have modelled this discrepancy in terms of a shift and a scaling applied to the dark matter predictions. For scales on which the fluctuations are weakly non-linear, the scaling can be identified with the linear bias, b_1, and the offset with the quadratic bias, b_2/b_1. Our best measurement of these bias parameters gives a linear bias consistent with unity, but a significant detection of a non-zero quadratic bias, $b_2/b_1 = -0.34^{+0.11}_{-0.08}$. This is the first time that the signature of a quadratic bias has been seen so convincingly; our measurements are 9σ away from the case in which galaxies faithfully trace the mass ($b_1 = 1$ and $b_2 = 0$). Our results disagree with some of the previous analyses of the three-point function in the 2dFGRS; a detailed discussion of the possible reasons for this is given in Section 5. We note that Feldman et al. (2001) also found a negative quadratic bias term when analysing the three-point function of galaxies in the *IRAS* PSCz survey, albeit at a less significant level than our detection.

The discrepancy between Q_3 for galaxies and the dark matter increases as the scale of the triangles is reduced (while remaining in the weakly non-linear regime), which translates into a slight increase in the best-fitting values of the bias parameters (see Table 2). We find no significance evidence for luminosity segregation on these weakly non-linear scales.

On smaller scales we are able to detect a significant dependence of Q_3 on scale, colour and luminosity. These trends appear at first sight to be at odds with the preliminary results obtained by Kayo et al. (2004) using the SDSS, although the errors on the measurements presented by these authors are much larger than ours. In all cases, the measurements for the various samples of galaxies are clearly below the predictions for the dark matter. Our detailed measurements, presented in Figs 6–8 and Table 3, should provide important new constraints on models of galaxy formation (see Scoccimarro et al. 2001b; Wang et al. 2004).

Our strong detection of a quadratic bias offers a new explanation of the long-standing puzzle of why redshift surveys have tended to measure a different skewness ($S_3^{\rm G} \sim \bar{\xi}_3/\bar{\xi}_2^2 = 2$; see Croton et al. 2004b for the 2dFGRS and table 19 of Bernardeau et al. 2002 for a summary of other observational results) from that predicted for the ΛCDM cosmology ($S_3^{\rm M} \sim 3$). If we take the non-linear bias relation derived by Fry & Gaztañaga (1993), $S_3^{\rm G} = (S_3^{\rm M} + 3c_2)/b_1$ and insert our best-fitting values for the bias parameters ($b_1 = 0.95$ and $c_2 = -0.35$), then we obtain $S_3^{\rm G} \simeq 2$, just as required by the observations.

The value of Q_3 is independent of the overall amplitude of fluctuations. This means that our measurement of the linear bias, b_1, is fully independent of the normalization of the fluctuations in the dark matter, as specified by σ_8. Furthermore, the predictions for Q_3 for dark matter are relatively insensitive to the shape of the power

[2] We note that such an analysis was, however, presented for Q_3 measured in Fourier space from the *IRAS* Point Source Redshift Catalogue (PSCz; Saunders et al. 2000) by Scoccimarro et al. (2001a) and Feldman et al. (2001).

[3] Note that this prediction differs from the hierarchical projection for the same model/scales estimated by Gaztañaga (1994), which were closer to $s_3 \simeq 4$. This was first noted by Bernardeau (1995) and later confirmed with simulations by Gaztañaga & Bernardeau (1998). See also comments relating to figs 47 and 54 in Bernardeau et al. (2002) for further details.

spectrum, making this estimate of the bias robust to minor changes in the parameters of the ΛCDM model. We can therefore combine our estimate of b_1 with the amplitude of fluctuations measured from the galaxy distribution, $\sigma_8^{\rm G}$, to derive an estimate of the amplitude of fluctuations in the dark matter, σ_8. Cole et al. (2005) measured the power spectrum of galaxy clustering in the 2dFGRS and found $\sigma_8^{\rm G} \simeq 0.924 \pm 0.032$. The equation relating fluctuations in the galaxies to those in the dark matter involves two other terms:

$$\sigma_8^{\rm G} = b_1\, D(z)\, K(\beta)\, \sigma_8. \tag{10}$$

Here $D(z) \simeq 0.95$ is the growth factor at the mean depth of the survey ($z \simeq 0.1$) relative to the growth factor at $z = 0$ and K is the linear Kaiser (1987) redshift space distortion factor: $K \simeq 1.17$ for $\beta \simeq 0.48$. Both factors depend on the cosmological density parameters for matter and vacuum energy, which we have set to their concordance model values ($\Omega_{\rm m} \simeq 0.3$, $\Omega_\Lambda \simeq 0.7$ and $h \simeq 0.7$). This allows us to estimate σ_8:

$$\sigma_8 \simeq 0.88^{+0.12}_{-0.10}. \tag{11}$$

Here we have assumed that the errors are dominated by the errors in b_1. This explains the good agreement found between the large-scale variance in 2dFGRS galaxies and the variance of the dark matter for $\sigma_8 \simeq 0.9$, as shown in fig. 2 of Baugh et al. (2004). A more detailed presentation of our result for σ_8 will be deferred to a later paper.

Note added on submission

On the day before our paper was submitted, Hikage et al. (2005) posted a paper on the three-point function of SDSS galaxies, in which they perform a Fourier phase analysis. Their main result is that $b_2/b_1 \approx 0$ if $\sigma_8 = 0.9$, in apparent contradiction with our principal finding. However, Hikage et al. consider scales in excess of $30\,h^{-1}$ Mpc and restrict their attention to triangles with large opening angles. Their analysis is therefore similar to the special case we present in Fig. 9 for elongated and equilateral triangles. As we explained in Section 4.3, in this case, due to the reduced number of triangles considered, the errors on the bias parameters are large. As shown in the upper-right panel of our Fig. 2, the error bars become quite large for $\alpha \simeq 180^\circ$ on large scales. Furthermore, there is actually no reason to expect the bias parameters extracted by Hikage et al. to agree closely with ours, as SDSS galaxies are red selected.

ACKNOWLEDGMENTS

We acknowledge discussions with Roman Scoccimarro, Cristiano Porciani, Pablo Fosalba, Alan Heavens and Licia Verde. EG acknowledges support from the Spanish Ministerio de Ciencia i Tecnologia, project AYA2002-00850 with EC-FEDER funding. PN is supported by an ETH Zwicky Fellowship. CMB is supported by a Royal Society University Research Fellowship. DC acknowledges the financial support of the International Max-Planck Research School in Astrophysics PhD fellowship. This work was supported by the EC's ALFA-II programme via its funding of the Latin American European Network for Astrophysics and Cosmology. The 2dFGRS was undertaken using the two-degree field spectrograph on the Anglo-Australian Telescope, and we thank the 2dFGRS Team for its release. The VLS and HV simulations in this paper were carried out by the Virgo Supercomputing Consortium using computers based at the Computing Centre of the Max-Planck Society in Garching and at the Edinburgh Parallel Computing Centre. The data are publicly available at http://www.mpa-garching.mpg.de/NumCos.

REFERENCES

Barriga J., Gaztañaga E., 2002, MNRAS, 333, 443
Baugh C. M. et al., 2004, MNRAS, 351, L44
Baumgart D. J., Fry J. N., 1991, ApJ, 375, 25
Benson A. J., Cole S., Frenk C. S., Baugh C. M., Lacey C. G., 2000, MNRAS, 311, 793
Berlind A. A. et al., 2003, ApJ, 593, 1
Bernardeau F., 1995, A&A, 301, 309
Bernardeau F., Colombi S., Gaztañaga E., Scoccimarro R., 2002, Phys. Rep., 367, 1
Bouchet F. R., Strauss M. A., Davis M., Fisher K. B., Yahil A., Huchra J. P., 1993, ApJ, 417, 36
Cole S., Hatton S., Weinberg D. H., Frenk C. S., 1998, MNRAS, 300, 945
Cole S. et al., 2005, MNRAS, 362, 505
Colless M. et al., 2001, MNRAS, 328, 1039
Colless M. et al., 2003, preprint (astro-ph/0306581)
Colombi S., Szapudi I., Szalay A. S., 1998, MNRAS, 296, 253
Conway E. et al., 2005, MNRAS, 356, 456
Croton D. J. et al., 2004a, MNRAS, 352, 828
Croton D. J. et al., 2004b, MNRAS, 352, 1232
Evrard A. E. et al., 2002, ApJ, 573, 7
Feldman H. A., Frieman J. A., Fry J. N., Scoccimarro R., 2001, Phys. Rev. Lett., 86, 1434
Fosalba P., Pan J., Szapudi I., 2005, ApJ, 632, 29
Frieman J. A., Gaztañaga E., 1994, ApJ, 425, 392
Frieman J. A., Gaztañaga E., 1999, ApJ, 521, L83
Fry J. N., 1994, Phys. Rev. Lett., 73, 2
Fry J. N., Gaztañaga E., 1993, ApJ, 413, 447
Fry J. N., Gaztañaga E., 1994, ApJ, 425, 1
Fry J. N., Peebles P. J. E., 1978, ApJ, 221, 19
Gaztañaga E., 1992, ApJ, 398, L17
Gaztañaga E., 1994, MNRAS, 268, 913
Gaztañaga E., Bernardeau F., 1998, A&A, 331, 829
Gaztañaga E., Frieman J. A., 1994, ApJ, 437, L13
Gaztañaga E., Scoccimarro R., 2005, MNRAS, 361, 824
Groth E. J., Peebles P. J. E., 1977, ApJ, 217, 385
Hawkins E. et al., 2003, MNRAS, 346, 78
Hikage C., Matsubara T., Suto Y., Park C., Szalay A. S., Brinkmann J., 2005, PASJ, in press (astro-ph/0506194)
Hoyle F., Szapudi I., Baugh C. M., 2000, MNRAS, 317, L51
Jing Y. P., Börner G., 1998, ApJ, 503, 37
Jing Y. P., Börner G., 2004, ApJ, 607, 140
Juszkiewicz R., Bouchet F. R., Colombi S., 1993, ApJ, 412, L9
Kaiser N., 1987, MNRAS, 227, 1
Kayo I. et al., 2004, PASJ, 56, 415
Lahav O. et al., 2002, MNRAS, 333, 961
Matarrese S., Verde L., Heavens A. F., 1997, MNRAS, 290, 651
Norberg P. et al., 2001, MNRAS, 328, 64
Norberg P. et al., 2002a, MNRAS, 332, 827
Norberg P. et al., 2002b, MNRAS, 336, 907
Pan J., Szapudi I., 2005, MNRAS, 362, 1363
Peacock J. A., Smith R. E., 2000, MNRAS, 318, 1144
Peebles P. J. E., 1980, The Large Scale Structure of the Universe. Princeton Univ. Press, Princeton, NJ
Peebles P. J. E., Groth E. J., 1975, ApJ, 196, 1
Percival W. J. et al., 2001, MNRAS, 327, 1297
Percival W. J. et al., 2002, MNRAS, 337, 1068
Sanchez A. G., Baugh C. M., Percival W. J., Peacock J. A., Padilla N. D., Cole S., Frenk C. S., Norberg P., 2005, MNRAS, submitted (astro-ph/0507583)
Saunders W. et al., 2000, MNRAS, 317, 55
Scoccimarro R., 1998, MNRAS, 299, 1097
Scoccimarro R., Feldman H., Fry J. N., Frieman J. A., 2001a, ApJ, 546, 652

Scoccimarro R., Sheth R. K., Hui L., Jain B., 2001b, ApJ, 546, 20
Scoccimarro R., Sefusatti E., Zaldarriaga M., 2004, Phys. Rev., D, 69, 103513
Sefusatti E., Scoccimarro R., 2005, Phys. Rev. D, 71, 063001
Szapudi I., Colombi S., Bernardeau F., 1999, MNRAS, 310, 428
Tegmark M. et al., 2004, Phys. Rev. D, 69, 103501
Verde L. et al., 2002, MNRAS, 335, 432
Wang Y., Yang X., Mo H. J., van den Bosch F. C., Chu Y., 2004, MNRAS, 353, 287
Wild V. et al., 2005, MNRAS, 356, 247
York D. G. et al., 2000, AJ, 120, 1579

This paper has been typeset from a TEX/LATEX file prepared by the author.